LINC

Learning about Interacting Networks in Climate

Marie Curie Initial Training Networks (ITN)

FP7- PEOPLE - 2011- ITN

Grant Agreement No. 289447

WorkPackage WP4: *Future Climate Change*

Deliverable D4.5

Report on near term projections of climate change

Marcelo Barreiro, Universidad de la República, Uruguay

Release date: 30 August 2015

Status: *public*

EXECUTIVE SUMMARY

One of the main objectives of the WP4 was to determine regime shifts in the evolution of the 20th century climate by analyzing reanalysis data and model simulations. In the Deliverable D4.2 we reported about our advances in understanding the influence of the global tropical oceans on precipitation over Southeastern South America (SESA) during spring time. The main finding was that this influence shows interdecadal variability and that different oceans play the most important role at different times of the 20th century, even though the equatorial Pacific dominates. Deliverable 4.3 reported on the evolution of the global atmospheric connectivity at upper levels during the 20th century. We found that the most connected areas are in the tropics and that the extratropical regions show a strong interdecadal variability in the connectivity. In Deliverable 4.4 we explore possible future changes in the influence of the tropical oceans on rainfall over SESA analyzing the output of CMIP5 models. We found that under a RCP8.5 scenario there will be a decrease of the synchronization among the tropical oceans and rainfall over SESA, suggesting that these oceans and SESA will become more disconnected in the future as consequence of anthropogenic forcing.

In his new Deliverable we now focus on understanding the processes that lead to the large interdecadal variability in rainfall over SESA. The characterization and understanding of variability on these time scales is crucial to be able to predict near term future climate changes as the anthropogenic forcing signal will still be within the range of internal climate variations. The study is divided into two complementary parts. In the first part we construct a climate network to detect synchronization periods among the tropical oceans and the precipitation over SESA. Afterwards, taking into account these results, we select two periods with different degree of synchronization to compare the spatial distribution of the moisture sources in order to estimate decadal variations. To do so we employ a Lagrangian particle dispersion model, that allows the calculation and tracking the trajectories of the atmospheric moisture.

Results show that during the last century there were three synchronization periods among the tropical oceans and the precipitation over SESA, which developed during the ‘30s, ‘70s and ‘90s decades. Comparison of moisture sources of SESA for the ‘80s (a non-synchronized period) and the ‘90s (a synchronized period) suggests that the main sources are the recycling over the region, the central-eastern shore of Brazil together with its surrounding Atlantic Oceans, and southwestern south Atlantic surrounding the SESA domain. The main differences the two selected decades (‘80s and ‘90s) are in the intensity of the recycling, in the intensity of the central-eastern shore of Brazil as a moisture source of SESA and in a region centered at 20ºS – 300ºE. The latter is a moisture source for SESA only during the ‘90s and could be associated with the development of a low-level anti-cyclonic anomaly circulation over central-east Brazil which favors the transport of moisture from the central Brazil toward SESA. On the other hand, during the ‘80s a low-level cyclonic anomaly circulation developed over the central-east Brazil favors a stronger advection of moisture from the central-eastern shore of Brazil toward the region of study. The strong decadal variability found (due to internal processes) is consistent with previous estimates and poses a challenge for predictions of near term climate change in the region.

Deliverable Identification Sheet

Grant Agreement No.	**PITN-GA-2011-289447**
Acronym	**LINC**
Full title	**Learning about Interacting Networks in Climate**
Project URL	http://climatelinc.eu/
EU Project Officer	Lucia PACILLO

Deliverable	**D4.5 Report on near term projections of climate change**
Work package	**WP4 Future Climate Change**

Date of delivery	**Contractual**	M 45	**Actual**	30-Aug-2015
Status	version. 1.00		final ☑	draft
Nature	Prototype	Report ☑	Dissemination	
Dissemination Level	Public	Consortium ☑		

Authors (Partner)	**Marcelo Barreiro, Universidad de la Republica, Uruguay**			
Responsible Author	Marcelo Barreiro		**Email**	barreiro@fisica.edu.uy
	Partner	Universidad de la República	**Phone**	

Abstract (for dissemination)	Report on the Deliverable 4.5 of WP4 of the LINC project.	
Keywords	Teleconnections, decadal climate variability, climate change	

TABLE OF CONTENTS

1 INTRODUCTION

Results from modelling studies using idealized experiments and CMIP5 models have shown that for South America the near term climate evolution will be strongly influenced by decadal variability, over which the climate change signal will develop. This has been also found in our studies using complex networks measures to address the role of the tropical oceans on south american climate. Thus, it is of outmost interest to characterize adequately the variability of climate on decadal time scales, and therefore we have focused our research on on this topic.

In particular, summertime is the season of rainfall for most of South America and one that shows large interannual and interdecadal variability. Within South America the subtropical region is subjected to large rainfall variations, due to interannual-decadal changes in circulation and in moisture sources. This study focuses on southeastern South America (SESA), a region that covers Uruguay and portions of northeastern Argentina and South Brazil. SESA is mostly located within La Plata Basin (LPB), the second largest basin in South America which comprehends parts of Brazil, Paraguay, Uruguay, Argentina and Bolivia. Located to the south of the Amazon basin, it is one of the most densely populated regions in South America. Moisture, precipitation and their variability are very important because they play a key role in the generation of hydroelectric energy and in the economy of these regions, which is mainly based on the harvesting and ranching (Berbery and Barros, 2002).

Moisture studies have focused mainly over the whole LPB and are described below. Moisture over LPB that could lead to future precipitations over the region can come from two different sources: (i) water vapor advection from others regions and/or (ii) local recycling. While the advection of water vapor depends on the atmospheric circulation and can have two different origins (continental or oceanic), the recycling is the process by which evapotranspiration from a particular continental region returns as precipitation to the same particular continental region (Brubaker et al., 1993). According to Martinez and Dominguez (2014), approximately 63% of the mean precipitation over La Plata Basin comes from South America and the remaining 37% comes mostly from the southern Pacific and Atlantic Oceans.

Previous studies have shown that the main continental moisture source of LPB by advection of water vapor is the Amazon Basin (e.g., Martinez and Dominguez 2014; Zemp et al., 2014; Drumond et al., 2014; Dirmeyer et al., 2009; Barros and Berbery 2002), contributing with 24% of the annual mean precipitation over LPB (Martinez and Dominguez, 2014). Using the concept of cascading moisture recycling, which represents the moisture transport between two locations on the continent that evolves one or more re-evaporation cycles along the way, Zemp et al., 2014 showed that the entire Amazon basin (northern plus southern parts of the Amazon basin) can be considered as an evaporative source of moisture for LPB, and moreover, that the southern part could act not only as the main direct continental moisture source of LPB but also as an intermediate region that distributes moisture originating from the entire Amazon basin during the wet season (December to March). The transport of the southern Amazonian moisture toward LPB takes place throughout the year, being a quasi-permanent source of moisture and with a maximum during the austral summer season (Berbery and Barros, 2002; Martinez and Dominguez 2014). The transport is carried out via the South American Low Level Jet (SALLJ) along the Andes (Marengo 2005; Martinez and Dominguez, 2014).

Another continental moisture source but without advection from other regions is the local recycling. For LPB, it represents the 23.5% of its total annual mean precipitation and becomes its maximum during the austral summer season due to the enhancement of the large-scale convergence and net radiation, which increase the atmospheric instability, precipitation and evaporation (Martinez and Dominguez 2014).

The Atlantic and Pacific oceans are the main oceanic moisture sources of LPB and are seasonally dependent (Drumond et al., 2008; Martinez and Dominguez 2014). Drummond et al., (2008) used a Lagrangian particle dispersion model to compute the trajectories of the particles in the atmosphere backwards in time. They found that the main oceanic moisture sources for LPB are the southwestern South Atlantic, the tropical north Atlantic and the surrounding Atlantic Ocean located eastern to central Brazil. While the two latter remain as moisture sources throughout the year, the moisture from the tropical north Atlantic only reaches LPB during the austral summer season. This is associated with the development of a cross equatorial flow carrying moisture from the north Atlantic that penetrates into South America. Over the continent, the presence of the Andes forces the flow to becomes northerly, and is channeled southwards reaching LPB (Drumond et al., 2008; Martinez and Dominguez 2014; Viviane et al., 2012).

Regarding the Pacific Ocean, Martinez and Dominguez (2014) showed that the subtropical and extratropical part of the south Pacific contributes to LPB precipitation with a 7.1% of the total annual mean precipitation, being its contribution more important during the austral winter.

It is well known that the atmospheric circulation is sensitive to the ocean surface conditions in the tropics. Anomalies in the surface temperatures (SST) over the tropical oceans are able to induce changes in the meridional circulation and also generate stationary Rossby waves that propagate from the tropics toward extratropical latitudes inducing variations in the atmosphere circulations patterns that induce rainfall variability (e.g., Grimm et al., 2000; Chan et al., 2008; Yoon and Zeng 2010; Silva et al., 2009, Barreiro and Tipmann, 2008; Martín-Gómez and Barreiro 2015). Moreover, circulation anomalies may result in changes in the sources of moisture (Castillo et al., 2014; Martinez and Dominguez 2014).

For the particular case of Southeastern South America (SESA), several previous studies have shown that the SST anomalies in the tropical Pacific, Atlantic and Indian oceans can influence precipitation variability through atmospheric teleconnections (e.g., Seager et al., 2010; Barreiro et al., 2014; Grimm et al., 2000; Silvestri, 2004; Barreiro, 2010; Diaz et al., 1998 and Chan et al., 2008) and also the moisture transport (e.g., Silva et al., 2009; Vera 2004; Martinez and Dominguez 2014; Castillo 2014).

El Niño-Southern Oscillation is one of the interannual variability phenomena that has been shown to influence the moisture transport from the Amazon Basin toward LPB through changes in the intensity of the SALLJ (Silva et al., 2009; Vera 2004; Martinez and Dominguez 2014). The physical mechanism through which the positive phase of El Niño induces an increase of the moisture of Amazonian origin in LPB involves a weakening of the Walker circulation that increases anomalous subsidence over Brazil which subsequently enhances upward motion over Southeastern South America (Andreoli and Kayano, 2005). This weakening in the local Hadley circulation between tropical and subtropical South America turns into a strengthens of the southward transport of moisture in lower levels from Brazil toward Southeastern South America,

which would be related to the increase number of SALLJ events during the positive phase of El Niño (Silva et al., 2009).

In turn, the warm phase of this equatorial Pacific phenomenon has been shown to increase the moisture from the southern Pacific in LPB (Martinez and Dominguez, 2014). Martinez and Dominguez (2014) suggest that this increase could be due to the anomalous upper-level circulation pattern during the Niño events, where stronger subtropical westerlies occur together with an anomalous cyclone located over the southern Pacific along with an anomalous anticyclone over the southern Atlantic (Andreaoli and Kayano, 2005; Vera et al., 2004; Ropelewski and Halpert, 1987).

Finally, the tropical oceans can interact with each other inducing sea surface temperature anomalies in remote basins through atmospheric and oceanic teleconnections (e.g., Alexander et al., 2002; Enfield and Mayer, 1997; Saravannan et al., 2000; Rodriguez-Fonseca et al., 2009; Yoo et al., 2013; Meyers et al., 2007; Annamalai et al., 2003; Wang and Wang, 2014; Wu and Kirtman, 2004). All the aforementioned studies focus on the impact of a particular ocean basin (or combination of two) on rainfall over SESA or on the surface ocean conditions of another basin. Recently Martín-Gómez and Barreiro (2015) used a methodology borrowed from complex networks to study how SST anomalies in the three tropical oceans can work together to induce rainfall variability over SESA. To our knowledge there are no studies that focus on how SST anomalies in the tropical oceans can together induce variability in the moisture sources of SESA at interdecadal time scales.

Thus, the aim of this study comprehends two parts: one first part in which following the methodology of Tsonis et al., (2007) and Martín-Gómez and Barreiro (2015), we construct a climate network in order to detect different synchronization periods among the tropical oceans and the precipitation over SESA during the last century. In the second part and taking into account the results from the former, we select two periods with different degree of synchronization and, employing a Lagrangian particle dispersion model, we calculate and compare the trajectories of the atmospheric moisture in both cases. This provides information about the spatial distribution of the moisture sources of Southeastern South America in the two selected periods and will provide a measure of the decadal variability of the region.

2 *CONSTRUCTION OF THE CLIMATE NETWORK*

A climate network is constructed considering as network's nodes the following five different tropical oceanic indices: El Niño3.4, Tropical North Atlantic (TNA), Tropical South Atlantic (TSA), Equatorial Atlantic (ATL3) and Indian Ocean Dipole (IOD), as well as a precipitation index over SESA (PCP SESA). The election of the indices takes into account all the tropical basins that are known to influence SESA precipitation during the austral summertime (see introduction). The oceanic indices are defined considering the monthly mean SST from the Extended Reconstructed Sea Surface Temperature database (ERSSTv3b; Smith *et al.*, 2008; and Xue *et al.*, 2003) with a resolution of 2º x 2º. The precipitation index is defined using the monthly mean observed data from the GPCCv5 (Global Precipitation Climatology Center; Schneider *et al.*, 2011) with a resolution of 1º x 1º. The period of study is 1901-2005.
We will also consider the monthly mean values of the vertical integral of the horizontal divergence of the moisture flux from ECMWF ERA-Interim reanalysis data, of the zonal and meridional winds at 850hPa and of the geopotential height at 200hPa obtained

from ECMWF data server (Dee *et al*. 2011). These fields are used to diagnose circulation anomalies and understand the changes in the moisture sources for SESA in different periods. The available data span the period 1979-to present, so we consider the common period (1979-2005). The methodology followed to construct the network is described in detail in Martín-Gómez and Barreiro (2015). Here we provide a summarized version. It consists in several steps:

- First, the climate indices are defined by spatially averaging the SST or precipitation anomalies in the respective regions (Table 1) within of individual trimesters: September – November (SON) for the case of El Niño3.4 index and December – February (DJF) for the other indices (TNA, TSA, ATL3, IOD and PCP).

  The lag time of 3 months among El Niño3.4 and the rest of the networks nodes was established in order to allow the rest of the nodes to respond to the atmospheric anomalies generated by the equatorial Pacific.

Index short name	Index long name	Earth's regions	
		Latitude range	**Longitude range**
NINO3.4	El Niño3.4	5ºN-5ºS	170ºW-120ºW
TNA	Tropical North Atlantic	10ºN-30ºN	60ºW-30ºW
TSA	Tropical South Atlantic	5ºS-25ºS	330ºE-358ºE
ATL3	Equatorial Atlantic	3ºN-3ºS	0ºW-20ºW
IOD	Indian Ocean Dipole	10ºS-10ºN	50ºE-70ºE
		10ºS-0ºN	90ºE-110ºE
PCP	Precipitation Southeastern South America (SESA). (only land areas are considered)	25ºS-40ºS	60ºW-50ºW

Table 1. Geographical regions of each index that make up our network's nodes. The indices are defined considering the spectral average of the sea surface temperature and precipitation anomalies in the specified regions. In the Indian Ocean Dipole case, the index is computed from the difference between the 2-D average SST in the west region and the 2-D average in the east region. Land areas are only considered for the case of the precipitation index.

- The climate network is constructed considering the mean network distance as a measure of synchronization among the nodes:

$$d(t) = \frac{2}{N(N-1)} \sum_{i<j} \sqrt{2\left(1 - \left|\rho_{ij}^{t}\right|\right)}$$

  where t denotes the time in the middle of a sliding window of width Δt=11 years, N represents the number of network's nodes (in this case, 6) and is the

correlation coefficient between nodes i and j in the interval [$t - \frac{\Delta t}{2}$, $t + \frac{\Delta t}{2}$].

Note that the network is completely synchronized when the distance is zero and disconnected when the distance is $\sqrt{2}$ (uncorrelated nodes).

- To compute the statistical significance of the mean network distance we employ the Montecarlo Method under the following criterion: we consider as red noise those nodes with autocorrelation coefficient at lag 1 significant at 95% level in a one-tailed t-test, in the opposite case as white noise. Following this criterion, only the TNA and TSA can be considered as a red noise. Then, we generate 1000 surrogate time series of each index under these null hypotheses and compute the network distance time series considering a sliding window of 11-years length. In this way, we construct 1000 surrogate time series of the mean network distance, which allows determining the 5% level. We consider that there is a statistically significant synchronization event when the mean network distance is below this threshold.
- In order to analyze the processes of rainfall variability over SESA in different periods, we represent the anomalous vertical integral of moisture flux divergence during DJF together with the anomalous eddy geopotential height at 200hPa (time anomaly of the zonal anomaly of the geopotential height) in the same season. These anomaly values were computed in the same way as done for the climate indices.

3 *DESCRIPTION OF LAGRANGIAN MODEL AND METHODOLOGY TO IDENTIFY THE MOISTURE SOURCES*

In order to get information about the spatial distribution of the moisture sources of Southeastern South America, we consider a Lagrangian particle dispersion model (FLEXPART, Sthol et al., 2005) driven by the 6 hours forecast from Climate Forecast System Reanalysis (NCEP-CFSR, Saha et al., 2010) with a resolution of 0.5º x 0.5º during the period 1979 to 2000. We consider the NCEP-CFSR data because as previous studies have shown, this reanalysis is able to reproduce correctly the lower and upper-level atmospheric circulation patterns and precipitation distribution over South America during the austral summer season (Viviane et al., 2012; Quadro et al., 2013).

FLEXPART is a Lagrangian Particle dispersion model able to calculate and track the trajectories of the atmospheric moisture running backward in time while dividing the atmosphere into a large number of particles (Stohl et al., 2005). Each particle represents one air mass with a specific mass (m) which is transported by the 3D winds field. In our work, the vertical distribution of the particles in the atmosphere is proportional to the air density and the moisture sources are computed through the net budget of evaporation minus precipitation obtained from the changes in the moisture along the particles trajectories. As in Sthol and James (2004, 2005) and in Drumond et al., (2008), the steps are:

- We first select the vertical atmosphere column located over SESA (see spatial domain on table 1), inside of which we release 50.000 particles per simulation with a vertical distribution proportional to the air density. We perform 5

simulations per month (December – January – February) releasing the particles the days: 12nd, 16th, 20th, 24th and 28th of each month. All these particles are transported by 3D winds backwards in time for 10 days over the period (1979-2000) and tracked recording their positions and specific humidity every 6 hours. We limit the transport of the particles to 10 days because, as previous studies have shown, it represents the average time that the water vapor resides in the atmosphere (Numagutti, 1999). In turn, we establish a lag time between consecutive simulations of 4 days in order to assure that the obtained particle trajectories are different in consecutives simulations, since the life time of the synoptic perturbation is around 5 days.

- Second, the net budget evaporation (e) minus precipitation (p) of each particle *i* was computed through changes in the specific humidity (q) along it trajectory:

$$(e - p)_i = \left[m \cdot \frac{dq}{dt} \right]_i$$

- Third, we define a (1º x 1º) grid and add $(e\text{-}p)_i$ for all the particles of the vertical column located over an area *A*, obtaining the net budget (E-P) for the whole vertical column of area *A* in each grid point:

$$(e - p)_i = \left[m \cdot \frac{dq}{dt} \right]_i \rightarrow (E - P) = \frac{\sum_{i;vertical\_column} (e - p)_i}{\rho \cdot Area_{column}}$$

- Fourth, the net budget (E-P) in each vertical column over an area *A* was computed for specific days. We call $(E\text{-}P)_n$ to the net budget evaporation minus precipitation of all the particles going toward SESA during the n-th day of trajectory, where n takes the values from 1 to 10 (which is time limit we run backwards in time the model in each simulation). Finally, we make the average of the 10 net budgets $(E\text{-}P)_n$, and call it $(E\text{-}P)^{10}$. Per each grid cell, the parameter $(E\text{-}P)^{10}$ will represent the net budget evaporation minus precipitation in the whole vertical column located over an area A (the area of the grid cell) averaged over the 10 days of trajectory of the particles going toward SESA. The positive (negative) values of $(E\text{-}P)^{10}$ will represent the regions where particles, in average over the 10 days of trajectory toward SESA, when passing gain (loss) moisture and therefore, these regions will represent sources of moisture (sink of moisture).

4 *CLIMATE NETWORK AND SYNCHRONIZATION PERIODS*

Figure 1 shows the network distance computed using Spearman correlation as the interdependency measure (black dashed line) and the PCP index on DJF (black line) during the last century. Regarding the mean network distance, the major features are:

(1) The network distance is characterized by interannual and interdecadal variability.

(2) During the last century there were three synchronization periods: (1934-1946), (1965-1975) and (1992-2000), marked by white bands in Figure 1.

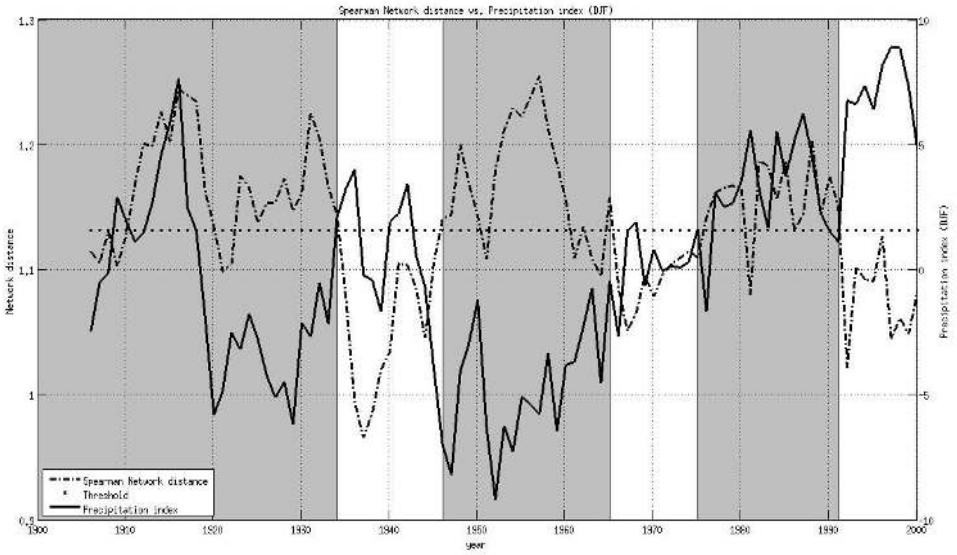

Figure 1. Mean network distance time series during the 20th century computed considering the Spearman correlation coefficient (dashed back curve). To compute this time series, Niño3.4 is centered on SON; TNA, TSA, ATL3, IOD and PCP are centered on DJF. The black line represents the precipitation index over SESA in austral summer and the horizontal black dot line represents the threshold level. Each point of the network distance time series represents the value of the mean network distance computed considering a sliding window of 11 years length.

The existence of synchronization periods indicates that several of the nodes in the network (or in the best case all of them) are interacting among them. However, this does not assure that during these periods the oceans are influencing rainfall over SESA. To address this question we compute the Spearman correlation coefficient between the mean network distance and a precipitation index over SESA constructed taking averages of 11 years windows. The resulting correlation coefficient, -0.25, is statistically significant at 5% significance level in one sided t-test (threshold level is 0.17), suggesting that an increase of the network distance (a decrease in the synchronization among the network's nodes) is associated with a decrease of the precipitation over SESA. The anti-correlation is evident in Figure 1. However, this result does not completely ensure the increment of SESA precipitation as consequence of enhancing the degree of synchronization of the network. To further address this issue we define the relative precipitation weight (RPW), a parameter that informs about the importance of the precipitation index as a network's node, understanding "importance" as the degree of interaction of the precipitation index with the rest of the network's nodes. The definition of RPW is:

$$RPW = \frac{\frac{\sqrt{2}}{3} - d_{pcp}}{\sqrt{2} - d}$$

where d_{pcp} represents the network distance calculated considering only the interaction between the precipitation index and the tropical oceanic indices in equation (1). The maximum and minimum values of the RPW are one and zero, in such a way that higher values of the RPW are associated with a larger influence of the tropical oceans on rainfall and vice versa. RPW=1 takes place when d_{pcp}=0 (correlation coefficient between

each one of the oceanic indices and PCP index are 1 or -1) and the tropical oceans are completely disconnected among them. RPW=0 means that SESA precipitation is completely disconnected from the tropical oceans indices.

The Spearman correlation coefficient between the RPW and the mean network distance, -0.22, is statistically significant at 5% significance level in a one sided t-test, suggesting that an increase of the connectivity of the precipitation index (increase of the RPW) is associated with a decrease of the network distance (increase of the synchronization of the network). On the other hand, we also computed the correlation coefficient between the RPW and the precipitation, obtaining the value 0.24, also statistically significant at 5% significance level in a one sided t-test. These results suggest that an increase of the precipitation in SESA is related to an increase of the tropical oceans influence on SESA, which in turn, is associated with the increase of the degree of synchronization.
So, one could conclude that overall an increase in the synchronization of the network is associated with an increase of the precipitation over SESA. Nevertheless, we note that there are periods in which precipitation is above normal but the network does not show synchronization, e.g. during the 80s (when considering the whole 20th century).

5 *MOISTURE SOURCES OF SESA DURING THE '80S AND '90S.*

To study decadal variability and given the availability of ERA Interim and NCEP-CFSR data, we focus our discussion on the differences between the '80s (1979-1991) and '90s (1992-2000), one period of non-synchronization and another of statistically significant synchronization among network's components. Note that reducing the period to 1979-2000, the '80s have rainfall below the mean, while the '90s have rainfall above the mean in SESA.

We first analyze SST and circulation anomalies in the two periods. The Spearman correlation map between the SESA precipitation index and the SST anomalies for the two periods, '80s and '90s are shown in Figure 2. The shaded regions are statistically significant at 5% significance level in a MonteCarlo test based on the generation of 100 surrogate time series. The first distinctive feature between these two decades is that while in the '90s the equatorial Pacific influences rainfall variability over SESA, during the '80s the equatorial Atlantic. The vertical integral of moisture flux divergence is consistent with increased rainfall over SESA during the 90s and decreased during the 80s (Figures 3(a) and (d)).

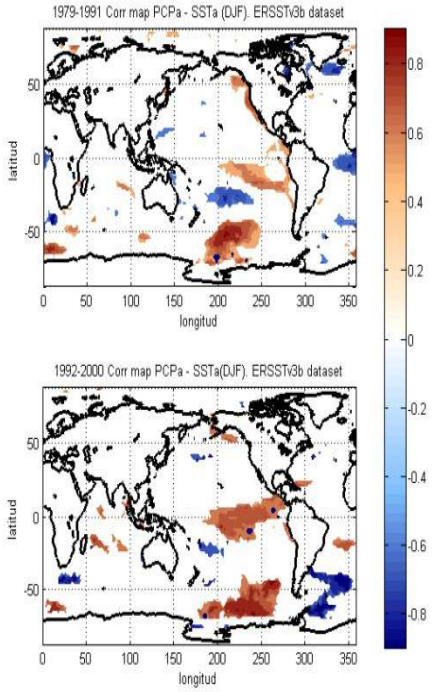

Figure 2. Spearman correlation maps PCP index and the SST anomalies centered on the austral summer season for (a) ‘80s decade and (b) ‘90s decade. The shaded domains represent those regions which are statistically significant at 95% significance level in a MonteCarlo test based on the generation of 100 surrogate time series.

Figure 3 (b) and (e) show the anomaly eddy geopotential height at 200mb during ‘80s and ‘90s respectively. The ‘80s are characterized by an anomalous anticyclone located southeast of South America over the Atlantic Ocean and an anomalous cyclone over southern South America (Figure 3(b)). This situation does not favor the convergence of moisture over SESA and inhibits vertical ascent motions. However, during the ‘90s the dipole cyclonic-anticyclonic in subtropical South America favors the advection of cyclonic vorticity and ascent motion over SESA, and therefore, the increase of the precipitation. The low level winds anomalies are consistent with this picture, showing mainly divergence (convergence) over SESA during the 80s (90s).

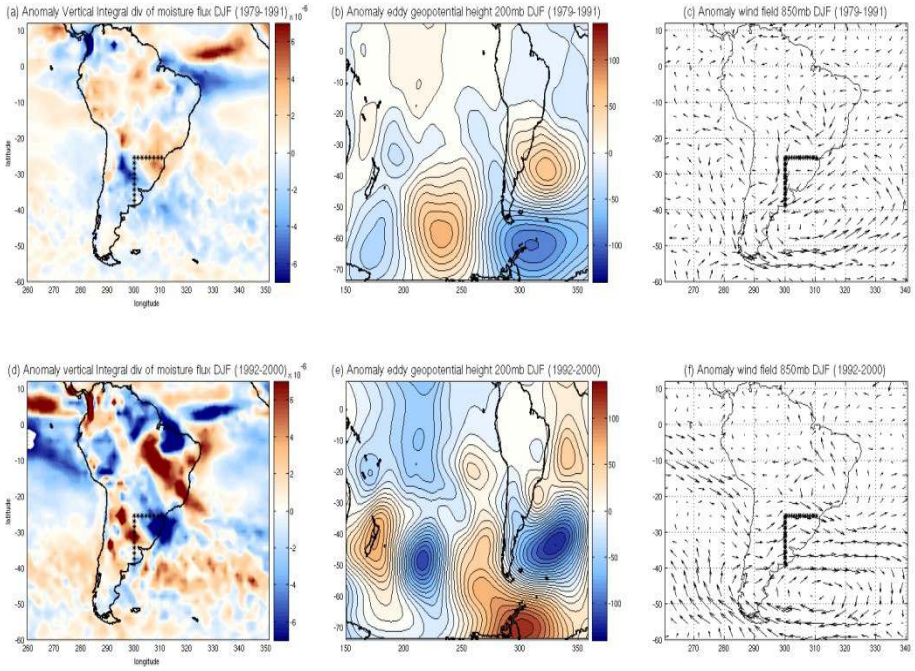

Figure 3. Anomaly eddy geopotential height (hgt) at 200mb for: (b) (1979-1991) and (e) (1992-2000). Anomaly vertical integral divergence moisture flux (Q) for: (a) (1979-1991) and (d) (1992-2000). Anomaly winds at 850mb for (c) (1979-1991) and (f) (1992-2000). To compute (b) and (e) maps, we first remove the trend and zonal average of the geopotential at 200mb. After that we remove the climatology and apply the low-pass the Lanczos filter to the time series. From this anomalies values we finally select DJF season and make an average for the periods: (1979-1991) and (1992-2000). To compute the (a), (d), (c) and (f) maps we remove the trend, the climatology and apply the Lanczos filter to the time series Then we compute the DJF average for each period to obtain the anomalies. The marked region over South America represents the domain where the PCP over SESA index was defined.

Figures 4 (a) and (b) represent the 10 days average of the net budget evaporation minus precipitation ($(E-P)^{10}$) over the periods (1979-1991) and (1992-2000), respectively. Regions with positive (negative) values of this variable are associated with a net profit (loss) of moisture of the particles when passing by along their trajectories toward SESA, and therefore, these regions will represent the main moisture sources (sinks) of SESA. From Figures 4 (a) and (b) we can see that the main moisture source regions (with positive values of the $(E-P)^{10}$) are: the recycling over SESA, the central-eastern shore of Brazil together with its surrounding Atlantic ocean, and the South Atlantic Ocean surrounding SESA shore. Results are almost in agreement with Figure 1 (d) from Drummond et al., 2008. The main difference arises over the central Brazil/Amazon basin, a region that in the previously mentioned study is characterized by positive values of the $(E-P)^{10}$ budget while in our case takes the opposite (negative values). The difference could be associated with the reanalysis data employed to drive the FLEXPART model: while we consider the NCEP-CFSR reanalysis, Drumond et al., 2008 employed a reanalysis from ECMWF. Other factors that can introduce differences are that the selected domain for SESA is not exactly the same and that we consider Dec-Jan-Feb, while Drumond et al., 2008 consider Jan-Feb-Mar season.

Figure 4 (c) plots the regions of the difference in $(E-P)^{10}$ during the 80s and 90s that are significant at 10% level. It shows that significant differences between both decades appear in the intensity of the net budget $(E-P)^{10}$ over the central-eastern shore of Brazil (being stronger during the 80s), in the presence of a positive region between 20ºS-25ºS at 300ºE during the 90s, and an increase in the intensity of the recycling over SESA in the 90s. The stronger intensity of the recycling over SESA during the 90s would be in agreement with the larger positive PCP anomalies observed on Figure 1 and the anomalous vertical integral of the moisture convergence shown in Figure 3(d).

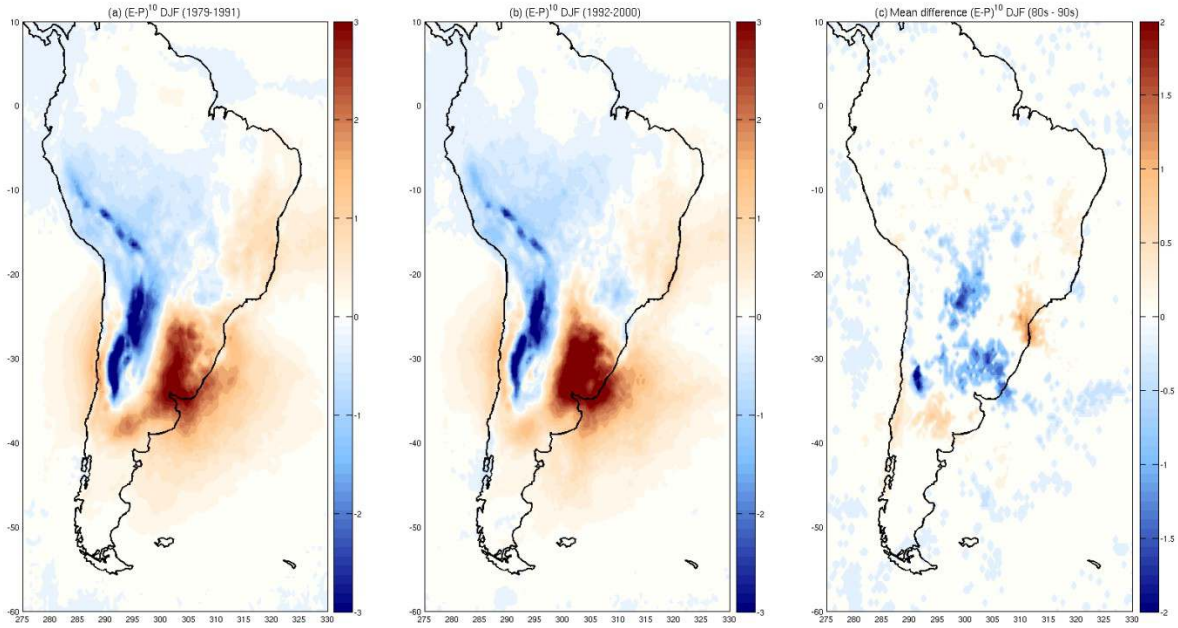

Figure 4. (a) 10 days average of the net budget evaporation minus precipitation ($(E-P)^{10}$) during the 80s (1979-1991) in DJF, (b) the same in the 90s (1992-2000) and (c) statistical significant difference between the 80s and 90s at 90% significance level considering a MonteCarlo approach.

To interpret the changes in the moisture sources we compute the Empirical Orthogonal Functions (EOFs) for the net budget $(E-P)^{10}$. Figure 5(a) shows the first EOF pattern that explains the 16.5% of the $(E-P)^{10}$ variance. Its associated PC is plotted on Figure 5(b). The EOF1 pattern shows a dipole-like structure with two centers of actions, one located over the central-eastern and southeast Brazil, and another one with opposite sign in the subtropical region located to the east of the Andes (20-35)ºS, (295-305)ºE. The associated PC1 shows a clear jump between both decades of study, '80s and'90s (see Figure 5(b)). Positive (negative) values of the PC1 tend to prevail before 1991 (after 1991) , suggesting that the center located over the central-eastern and southeast Brazil would take positive (negative) values, and therefore, the particles that pass through that region along their trajectory toward SESA will load more (less) moisture. This center of action is associated with the statistically significant positive signal observed on Figure 4(c) over the central-eastern and southeast Brazil. The other center of action of the EOF1 pattern would have the opposite sign and could be related to the two statistically significant negative signals observed in Figure 4(c) over the subtropical region located to the east of the Andes. The stronger intensity of low level winds in central-eastern and southeast shores of Brazil suggests that it might be the transport of moisture from there

toward SESA during the ‘80s. This flow is caused of enhanced further strengthened by low-level anomalous cyclonic circulation centered at (15ºS, 310ºE) during the 80s (Figure 3 (c)). During the 90s the situation is the opposite, the low-level anti-cyclonic circulation developed over the central-east Brazil does not favor the advection of moisture from the central-east shore of Brazil toward SESA, decreasing the contribution of this region as a moisture source to SESA precipitation. Note that the development of this low-level cyclonic (anti-cyclonic) anomaly circulation over the central-east Brazil during the ‘80s (‘90s) is, in turn, consistent with the observed convergence anomaly of the vertical integral of moisture flux over the region shown in Figure 3(a) (Figure 3(d)).
The low-level anti-cyclonic anomaly circulation that develops over the central-eastern Brazil during the 90s favors the advection of moisture from the Amazon Basin toward SESA. This explains the extension of the region of moisture source toward the north of SESA in that decade.
Thus, overall, during the 90s there is an increase in cyclonic vorticity advection in upper levels and a strong contribution of moisture from the Amazon at lower level, resulting in an increase of the precipitation in SESA with respect to the 80s.

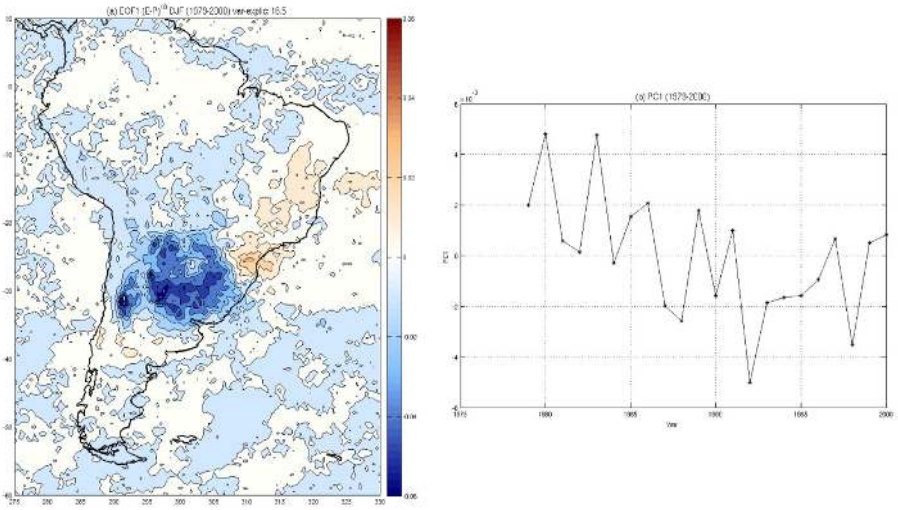

Figure 5. (a) First EOF of (E-P)[10] and (b) its associated PC1. Period (1979-2000).

6 *SUMMARY*

The atmosphere is sensitive to the ocean surface conditions in the tropics in such a way that sea surface temperatures (SST) anomalies over the tropical oceans are able to generate quasi-stationary Rossby waves that propagate from the tropics toward extratropical latitudes inducing regional circulation anomalies that can not only induce rainfall variability, but also changes in the sources of moisture. The work reported here is divided in two complementary parts: in the first part we construct a climate network to detect synchronization periods among the tropical oceans and the precipitation over Southeastern South America (SESA) during the austral summer season. Afterwards, taking into account these results, we select two periods with different degree of synchronization to compare the spatial distribution of the moisture sources. To do so we

employ a Lagrangian particle dispersion model, that allows the calculation and tracking the trajectories of the atmospheric moisture.

Results show that during the last century the network distance was characterized by interannual and interdecadal variability having three synchronization periods among the tropical oceans and the precipitation over SESA, which developed during the ‘30s, ‘70s and ‘90s decades. The relationship between the mean network distance and the precipitation over SESA is such that an increase of the degree of synchronization among the network’s component (decrease of the mean network distance) is associated with an increase of the oceanic influence on SESA precipitation.

We then focus on the differences between the ‘80s (1979-1991) and the ‘90s (1992-2000), one period of non-synchronization and another of statistically significant synchronization among the tropical oceans and SESA precipitation. The comparison yielded the following conclusions:

a. When the synchronization of the network is statistically significant (‘90s) there is convergence of moisture and favoring conditions for ascent motions over SESA, allowing an increase of the SESA precipitation. The opposite conditions can be observed in the period of non-synchronization (‘80s) resulting in reduced rainfall.

b. The main moisture sources of SESA are the recycling over the region, the central-eastern shore of Brazil together with its surrounding Atlantic Ocean, and the southwestern south Atlantic surrounding the SESA domain.

c. Comparison of the moisture sources for the ‘80s (a non-synchronized period) and ‘90s (a synchronized period) suggests that the main differences between the two selected decades are in the intensity of the recycling, in the intensity of the central-eastern shore of Brazil as a moisture source of SESA and in a region centered at 20ºS – 300ºE. The latter is a moisture source for SESA only during the ‘90s and could be associated with the development of a low-level anti-cyclonic anomaly circulation over central-east Brazil which favors the transport of moisture from that region toward SESA. On the other hand, during the ‘80s a low-level cyclonic anomaly circulation developed over central-east Brazil favoring a stronger advection of moisture from the central-eastern shore of Brazil toward the region of study.

7 REFERENCES

Alexander M, Blade AI, Newman M, Lanzante JR, Lau N-C, Scott JD (2002) The atmospheric bridge: the influence of ENSO teleconnections on air–sea interaction over the global oceans. J Clim 15:2205–2231.

Andreoli, R. V., & Kayano, M. T. (2005). ENSO-related rainfall anomalies in South America and associated circulation features during warm and cold Pacific decadal oscillation regimes. *International Journal of Climatology*, *25*(15), 2017-2030.

Annamalai H, Murtugudde R, Potemra J, Xie SP, Liu P, Wang B. 2003. Coupled dynamics over the Indian Ocean: spring initiation of the zonal mode. *Deep Sea Research II:Tropical Studies in Oceanography*, **50**(12): 2305-2330.
Barreiro, M., and Tippmann, A. 2008. Atlantic modulation of El Nino influence on summertime rainfall over southeastern South America. *Geophysical Research Letters*, *35*(16).

Barreiro M. 2010: Influence of ENSO and South Atlantic Ocean on climate predictability over southeastern South America. *Climate dynamics **35**: 1493-1508.* DOI: 10.1007/s00382-0666-9

Barreiro M, Diaz N, Remon M. 2014. Role of the oceans and land-atmosphere interaction on summertime interdecadal variability over northern Argentina. *Climate dynamics.* DOI: *10.1007/s00382-014-2088-6*

Berbery, E. H., & Barros, V. R. (2002). The hydrologic cycle of the La Plata basin in South America. *Journal of Hydrometeorology*, *3*(6), 630-645.

Brubaker, K. L., Entekhabi, D., & Eagleson, P. S. (1993). Estimation of continental precipitation recycling. *Journal of Climate*, *6*(6), 1077-1089.

Castillo, R., Nieto, R., Drumond, A., & Gimeno, L. (2014). The role of the ENSO cycle in the modulation of moisture transport from major oceanic moisture sources. Water Resources Research, 50(2), 1046-1058.

Chan SC, Behera SK, Yamagata T. 2008. Indian Ocean Dipole influence on South American rainfall. *Geophysical Research Letters* **35**(14). DOI: 10.1029/2008GL034204.
Dee DP, Uppala SM, Simmons AJ, Berrisford P, Poli P, Kobayashi S, Andrae U, Balmaseda MA, Balsamo G, Bauer P, Bechtold P, Beljaars ACM, van de Berg L, Bidlot J, Bormann N, Delsol C, Dragani R, Fuentes M, Geer AJ, Haimberger L, Healy SB, Hersbach H, Holm EV, Isaksen L, Kallberg P, Kohler M, Matricardi M, McNally AP, Monge-Sanz BM, Morcrette J-J, Park B-K, Peubey C, de Rosnay P, Tavolato C, Thepaut J-N, Vitart F. 2011. The ERA Interim reanalysis: Configuration and performance of the data assimilation system. *Quarterly Journal of the Royal Meteorological Society*, *137*(656), 553-597.

Diaz AF, Studzinski CD, Mechoso CR. 1998. Relationships between precipitation anomalies in Uruguay and southern Brazil and sea surface temperature in the Pacific and Atlantic Oceans. *Journal of Climate* **11**(2): 251-271.
Dirmeyer, P. A., Brubaker, K. L., & DelSole, T. (2009). Import and export of atmospheric water vapor between nations. *Journal of hydrology*, *365*(1), 11-22.

Drumond, A., Marengo, J., Ambrizzi, T., Nieto, R., Moreira, L., & Gimeno, L. (2014). The role of the Amazon Basin moisture in the atmospheric branch of the hydrological cycle: a Lagrangian analysis. *Hydrology and Earth System Sciences*, *18*(7), 2577.

Drumond, A., Nieto, R., Gimeno, L., & Ambrizzi, T. (2008). A Lagrangian identification of major sources of moisture over Central Brazil and La Plata Basin. *Journal of Geophysical Research: Atmospheres (1984–2012)*, *113*(D14).

Enfield DB, Mayer DA. 1997. Tropical Atlantic sea surface temperature variability and its relation to El Niño Southern Oscillation. *Journal of Geophysical Research: Oceans.* **102**: 929-945. DOI: 10.1029/96JC03296.

Grimm AM, Barros VR, Doyle ME. 2000. Climate variability in Southern South America associated with El Niño and La Niña events. *Journal of Climate* **13**(1): 35-58.
Quadro, M. F., Berbery, E. H., Dias, M. S., Herdies, D. L., & Gonçalves, L. G. (2013, May). The atmospheric water cycle over South America as seen in the new generation of global reanalyses. In *AIP Conference Proceedings* (Vol. 732, pp. 732-735).

Marengo, J. A. (2005). Characteristics and spatio-temporal variability of the Amazon River Basin Water Budget. *Climate Dynamics*, *24*(1), 11-22.

Martín-Gómez V and Barreiro M (2015). Analysis of ocean's influence on spring time rainfall variability over southeastern South America during the 20th century *Int. J. Climatology, in press*

Martinez, J. A., & Dominguez, F. (2014). Sources of Atmospheric Moisture for the La Plata River Basin*. *Journal of Climate*, *27*(17), 6737-6753.

Meyers G, Mcintosh P, Pigot L, and Pook M. 2007. The years of El Niño, La Niña and Interactions with the Tropical Indian Ocean. *Journal of Climate* **20**: 2872-2880.
Nogués-Paegle, J., & Mo, K. C. (1997). Alternating wet and dry conditions over South America during summer. *Monthly Weather Review*, *125*(2), 279-291.

Numaguti, A. (1999). Origin and recycling processes of precipitating water over the Eurasian continent: Experiments using an atmospheric general circulation model. *Journal of Geophysical Research: Atmospheres (1984–2012)*, *104*(D2), 1957-1972.

Rodriguez-Fonseca B, Polo I, Garcia-Serrano J, Losada T, Mohino E, Mechoso CR, Kucharski F. 2009. Are Atlantic Niño enhancing Pacific ENSO events in recent decades? *Geophysical Research Letters*. **36**(20): L20705. DOI: 10.1029/2009GL040048.

Ropelewski, C. F., & Halpert, M. S. (1987). Global and regional scale precipitation patterns associated with the El Niño/Southern Oscillation. *Monthly weather review*, *115*(8), 1606-1626.

Saha, S., et al. 2010. NCEP Climate Forecast System Reanalysis (CFSR) 6-hourly Products, January 1979 to December 2010. Research Data Archive at the National Center for Atmospheric Research, Computational and Information Systems Laboratory. http://dx.doi.org/10.5065/D69K487J.

Saravanan R, and Chang P. 2000. Interaction between Tropical Atlantic Variability and El Niño – Southern Oscillation. *Journal of Climate* **13**: 2177-2194.

Schneider U, Becker A, Finger P; Meyer-Christoffer A, Rudolf B, Bruno; Ziese M. 2011. GPCC Full Data Reanalysis Version 6.0 at 1.0: Monthly Land-Surface Precipitation from Rain-Gauges built on GTS-based and Historic Data. DOI: 10.5676/DWD_GPCC/FD_M_V6_100.

Seager R, Naik N, Baethgen W, Robertson A, Kushnir Y, Nakamura J, Jurburg S. 2010. Tropical Oceanic Causes of Interannual to Multidecadal Precipitation Variability in Southeast South America over the past Century. *Journal of Climate*. 23: 5517-5539. Doi: 10.1175/2010JCLI3578.1.

Silva, G. A., Ambrizzi, T., & Marengo, J. A. 2009. Observational evidences on the modulation of the South American Low Level Jet east of the Andes according the ENSO variability. In *Annales geophysicae* (Vol. 27, No. 2, pp. 645-657). Copernicus GmbH.

Silvestri GE. 2004. El Niño signal variability in the precipitation over southeastern South America during the austral summer. *Geophysical Research Letters* **31**(18). DOI: 10.1029/2004GL020590.

Smith TM, Reynolds RW, Peterson TC, Lawrimore J. 2008. Improvements to NOAA's Historical Merged Land-Ocean Surface Temperature Analysis (1880-2006). *Journal of Climate.*, **21,** 2283-2296.

Stohl, A., Forster, C., Frank, A., Seibert, P., & Wotawa, G. (2005). Technical note: The Lagrangian particle dispersion model FLEXPART version 6.2. *Atmospheric Chemistry and Physics*, *5*(9), 2461-2474.

Stohl, A., and P. James (2004), A Lagrangian analysis of the atmospheric branch of the global water cycle. part I: Method description, validation, and demonstration for the August 2002 flooding in central Europe, J. Hydrometeorol., 5, 656–678.

Stohl, A., and P. James (2005), A Lagrangian analysis of the atmospheric branch of the global water cycle. part II: Earth's river catchments, ocean basins, and moisture transports between them, J. Hydrometeorol., 6, 961–984.

Tsonis AA, Swanson K, Kravtsov S. 2007. A new dynamical mechanism for major climate shifts. *Geophysical Research Letters* **34**(13): L13705. DOI: 10.1029/2007GL030288.

Vera, C., Silvestri, G., Barros, V., & Carril, A. (2004). Differences in el nino response over the southern hemisphere. *Journal of climate*, *17*(9), 1741-1753.

Vera, C., Higgins, W., Amador, J., Ambrizzi, T., Garreaud, R., Gochis, D., ... & Zhang, C. (2006). Toward a unified view of the American monsoon systems. *Journal of Climate*, *19*(20), 4977-5000.

Viviane B. S. Silva and Vernon E. Kousky (2012). The South American Monsoon System: Climatology and Variability, Modern Climatology, Dr Shih-Yu Wang (Ed.), ISBN: 978-953-51-0095-9, InTech, DOI: 10.5772/38565. Available from: http://www.intechopen.com/books/modern-climatology/the-south-american-monsoon-system-climatology-and-variability

Wang X, and Wang C. 2014. Different impacts of various El Niño events on the Indian Ocean Dipole. *Climate dynamics* **42**: 991-1005

Wu R, Kirtman BP. 2004. Understanding the Impacts of the Indian Ocean on ENSO Variability in a Coupled GCM. *Journal of Climate* **17**: 4019-4031.
Xue, Y, Smith TM, Reynolds RW. 2003. Interdecadal changes of 30-yr SST normal during 1871-2000 *Journal of Climate*, **16**, 1601-1612.
Yoo GH, Kug JS, Park JY, Jin FF. 2013. Sea surface temperature in the north tropical Atlantic as a trigger for El Niño/Southern Oscillation events. *Nature Geoscience* 6:112-116. Doi: 10.1038/NGEO1986.

Yoon, J. H., & Zeng, N. (2010). An Atlantic influence on Amazon rainfall. Climate dynamics, 34(2-3), 249-264.

Zemp, D. C., Schleussner, C. F., Barbosa, H. M. J., Van der Ent, R. J., Donges, J. F., Heinke, J., ... & Rammig, A. (2014). On the importance of cascading moisture recycling in South America. *Atmospheric Chemistry and Physics*, *14*(23), 13337-13359.